DC Fault Detection in Meshed MTDC Systems Based on Transient Average Value of Current

Yujun Li, Jiapeng Li, Liansong Xiong, *Member, IEEE,* Xian Zhang,
and Zhao Xu, *Senior Member, IEEE*

Abstract—It is of great significance for voltage source converter (VSC) based multi-terminal DC (MTDC) grid to isolate the DC fault lines within several milliseconds after DC fault. Existing protection schemes and fault analysis methods are mainly based on the numerical simulations, which are lack of the theoretical analysis. In this paper, a high-frequency equivalent model of VSC based MTDC grid that is utilize for initial DC fault current calculation is firstly proposed. In the proposed model, the parallel connected capacitors of VSCs are regarded as short-circuited, and the initial fault current calculation of the fault DC line and the healthy DC line can be reduced as a simplified *RL* and *RLC* circuit. Accordingly, a novel DC fault detection method for VSC based MTDC system is further proposed. In the proposed approach, the primary detection utilizes the transient average value of line current and the fault DC line can be identified quickly with only one-end information. In addition, the errors between the transient fault current calculation based on the distributed parameters line model and the lumped parameters line model are also evaluated. Numerous simulation studies carried out in PSCAD/EMTDC have demonstrated that the proposed high-frequency equivalent model can be utilized for initial DC fault analysis of VSC-MTDC system and the proposed protection scheme is effective under different fault locations and high fault resistances. Compared with the traditional protection schemes based on rate of change of current (ROCOC), the proposed one requires relatively low sampling frequency, low computation burden, and has high fault resistance tolerant ability, and high robustness with respect to the data missing.

Y. Li is with the School of Electrical Engineering, Xi'an Jiaotong University. He is also with the Department of Electrical Engineering, The Hong Kong Polytechnic University, Hong Kong (email: yujunlizju@gmail.com).

J. Li is with the School of Electrical Engineering, Xi'an Jiaotong University (email: wennuanfrank@gmail.com).

L. Xiong is with the School of Automation, Nanjing Institute of Technology. He is also with the Department of Electrical Engineering, The Hong Kong Polytechnic University, Hong Kong (email: xiongliansong@163.com).

X. Zhang and Z. Xu are with the Department of Electrical Engineering, The Hong Kong Polytechnic University, Hong Kong. (e-mail: xian_zhang1988@163.com, eezhaoxu@polyu.edu.hk)

Index Terms—Fault current analysis, high frequency equivalent model, VSC based MTDC, transient travelling-wave.

I. INTRODUCTION

RECENTLY, the voltage source converter (VSC) based high voltage direct current (HVDC) system has been widely applied in the integration of large amount of renewable energy and the interconnection of asynchronous network [1]. A multi-terminal DC grid (MTDC) system that connects multiple converters with DC lines in meshes or radials [2] is considered as one of the best solutions for connecting large-scale of fluctuating renewables with different positions over long distances. One feasible project currently under envisaged is European "Super Grid" [3] that utilizes MTDC grid to transmit large-scale offshore wind energy into the European mainland. One of major challenges for the future development of DC gird is the fault current calculation and detection in a mesh MTDC grid [4-14].

A. Related works

Short-circuit current calculation and analysis is crucial for the power system and protection design. For the fault current calculation of MTDC system, [4] and [5] deduced the analytical equation for single terminal HVDC system, which is not suitable for the fault current calculation in the multi-terminal system since the mutual coupling of each converter should be considered in the fault analysis. References [6] and [7] presents the DC fault analysis of two-level VSC and MMC based MTDC system. However, the results are mainly based on the electromagnetic transient (EMT) simulations, which is quite time-consuming when the DC network is large and complex. In addition, the simulations can only provide the information by several classical scenarios. A generic fault current calculation algorithm for DC grid proposed in [8] establishes the fault matrix of the entire DC grid. However, this method can not give the clear analytical expression of the fault current nor the parameters that influence the fault current.

In terms of the protection schemes for HVDC system, current differential method [9] is a one of ideal ways to achieve fault detection with high selectivity. However, it requires the information from both sides of DC lines. The communication delay due to the long line may not be suitable for fast primary protection in a DC grid. In order to improve DC fault detection

performance, transient components are widely utilized for the protection design [10]. Using transient harmonic current relying on a single-frequency component for point to point HVDC system is proposed in [11, 12]. However, this method is vulnerable to be disturbed by outside noises, and may not be suitable for MTDC system since multi resonance frequencies exist during DC faults in the system. Another method that achieves fast fault detection is based on the current or voltage derivative [13]. However, high-frequency sampling is required and it is rather sensitive to the fault resistance.

Recently, the DC reactors [14] connected at the end of each DC line are widely utilized for limiting the DC fault current, and it can be regarded as a useful means for fast DC protection. Reference [15] uses the rate of change of the voltage measured across the DC reactor, and [16] utilizes the DC reactor voltage for identifying the fault line in 2 ms or less. Reference [17] uses high frequency voltage components of DC reactor voltage by calculating the ratio of the transient voltages at both side of inductor. Existing methods [15-17] are mainly based on detecting the transient components on the DC reactors at the end of each lines, which add new measurement equipment and lower the reliability of the protection.

Above rate of change of current or voltage (ROCOC or ROCOV) based methods [13-17] normally require extremely high sampling frequency (up to hundreds of kHz or 1MHz) so that the first reflection of the current/voltage travelling-wave can be captured. However, in the practical engineering, the primary protection relay will be activated by detecting three or four continuous ROCOC or ROCOV that are over the set threshold. As a result, the traditional methods are vulnerably invalid when the sampling frequency is relatively low, or missing some first few data of initial DC fault current.

B. Main contribution

To overcome foreheads shortcomings, main contributions of this paper lie on two folds. On one hand, most existing literatures focus on the fault analysis of MTDC system based on the numerical simulations and forming complex fault matrix, resulting in the fault current analytical expression not clearly presented. Therefore, this paper firstly proposed a simplified high-frequency equivalent model of MTDC grid, which can be utilized for DC fault current calculation. In the proposed model, the parallel connected capacitors of VSCs are regarded as short-circuited, and the initial fault current calculation of the fault DC line and the healthy DC line can be reduced as a simplified RL and RLC circuit. It is well verified from the theoretical and simulation results that the fault current components of fault line increase linearly, while that of healthy line raises cubically in the initial period of DC fault.

On the other hand, a novel DC fault detection method for VSC based MTDC system is further proposed. Based on the DC fault current component discrimination of fault DC line and healthy DC line, the transient average value of current is utilized as a primary protection indicator for DC fault detection and the fault DC line can be quickly identified using one-end information. In addition, the influence of the transient traveling-wave appearing in the long-transmission line on the

proposed protection scheme is also investigated. Compared with the traditional protection schemes based on ROCOC, the proposed one stands out for relatively low sampling frequency, high fault resistance tolerant ability, and high robustness with respect to the data missing.

II. DC FAULT CURRENT CALCULATION IN MTDC SYSTEM

A. Typical topology of MTDC system

In a meshed DC grid, fault DC line should be accurately identified in several milliseconds for DC circuit breaker (CB) to operate after a DC short-circuit fault. Therefore, the DC current within the initial period after fault may be the concern of the power system protection design. When a pole-to-ground DC fault occurs, the parallel connected capacitors of VSC begin to discharge and the fault current surges dramatically. Meanwhile, during the initial short period after fault, the VSC can still be regarded as a current-controlled source due to the small drop of DC-link voltage, and the fault component from AC side source can be ignored for the initial period of DC fault analysis. Therefore, the VSC can be simply regarded as the parallel connected capacitors in the following analysis.

A typical three-terminal DC grid that incorporates a solid pole-to-ground DC fault at the Line 12 is shown in Fig. 1. The supplemental inductor at DC side is usually implemented to reduce the DC current ripple, as the same effect as the smoothing reactor in the LCC based HVDC. Recently, in order to limit the peak value and the rising rate of the DC fault current, large inductor with several hundreds of mH is applied in MTDC grid so that DC CB can interrupt the fault current in several milliseconds. In order to facilitate the analysis, the DC overhead lines are approximated as series RL circuits, and the DC fault current calculation error with different line models involved will be further discussed in Section IV. R_{mk} and L_{mk} are the resistance and inductance of the Line mk. R_{m0} and L_{m0} are the resistance and inductance to the fault location from side m. L_{Tmk} is the DC supplemental inductor at the m side of branch mk. C_{cm} is the DC-link capacitance of VSCm.
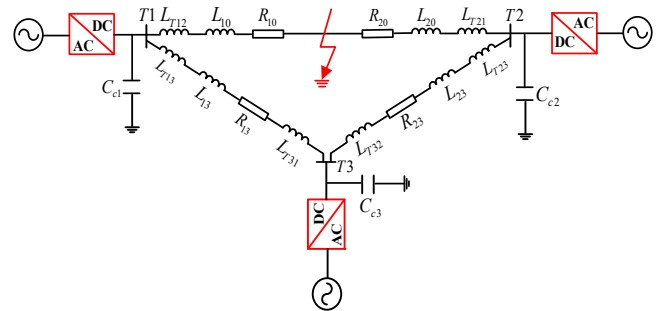

Fig. 1. RLC circuit of the typical three-terminal DC grid.

B. Calculation of short-circuit DC current

Since the steady-state component can be negligible compared to the fault current component, only fault component of DC line current is considered in the following analysis. According to the superposition principle, the fault component of DC current can be calculated by solving the passive network with only one fault DC voltage source U_0. In order to facilitate
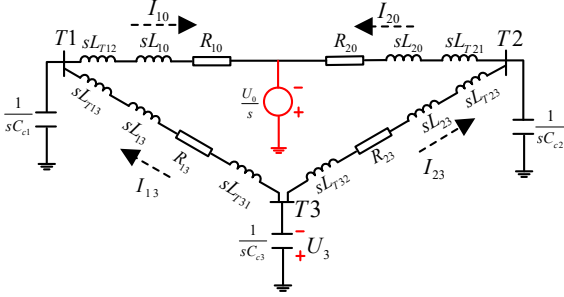
Fig. 2. Laplace circuit transformation of the studied three-terminal DC network for calculating the fault component.

the analysis, the positive direction of DC line current is from the healthy line to the fault line. Fig. 2 shows the Laplace circuit transformation of the studied three-terminal DC network for calculating the fault current component. The DC-link capacitor voltage of Terminal 3 can be expressed as follows:

$$U_3(s) = (I_{13}(s) + I_{23}(s))/sC_{c3} \qquad (1)$$

where, U_3 is the DC-link capacitor voltage of the Terminal 3. I_{13}, I_{23} are the DC line current of Line 13 and 23, respectively. In order to facilitate the calculation, the DC-link capacitor branch of Terminal 3 can be decoupled into two independent capacitors, which belong to Line 13 and 23. The corresponding impendence Z_{c13}, Z_{c23} should be satisfied as follows,

$$\begin{cases} Z_{c13}(s) = \dfrac{(I_{13}(s) + I_{23}(s))/sC_{c3}}{I_{13}(s)} \\ Z_{c23}(s) = \dfrac{(I_{13}(s) + I_{23}(s))/sC_{c3}}{I_{23}(s)} \end{cases} \qquad (2)$$

Define the proportional coefficient of DC fault current of Line 13 and Line 23 as follows:

$$k = I_{23}(s)/I_{13}(s) \qquad (3)$$

where, k is correlated proportional coefficient and it is related with the fault location of the Line 12, the length of the transmission Line 23 and 13, and the inductance of the supplementary inductor. The capacitance of two independent capacitors marked as C_{c13} and C_{c23}, which belong to Line 13 and 23 can be expressed as follows,

$$\begin{cases} C_{c13} = C_{c3}/(1+k) \\ C_{c23} = \dfrac{C_{c3}}{1+1/k} \end{cases} \qquad (4)$$

Accordingly, the meshed MTDC system can be unlocked into two independent radical networks shown in Fig. 3. Therefore, the fault current component of the fault line I_{10} can be expressed as follows,

$$I_{10}(s) = \frac{U_0/s}{R_{10} + s(L_{10} + L_{T12}) + Z_{f10}(s)}$$

$$Z_{f10}(s) = 1/sC_{c1} \cdot \frac{s(L_{13} + L_{T13} + L_{T31}) + 1/sC_{c13} + R_{13}}{s(L_{13} + L_{T13} + L_{T31}) + 1/sC_{c1} + 1/sC_{c13} + R_{13}} \qquad (5)$$

where, Z_{f10} is the total impendence of the DC-link capacitor of Terminal 1 parallel connected with branch Line 13.

C. High frequency equivalent model

It is very difficult to get the mathematic expression of $I_{10}(t)$ based on the *Inverse Laplace Transform* of (5). Therefore, an equivalent model should be put forward to obtain an
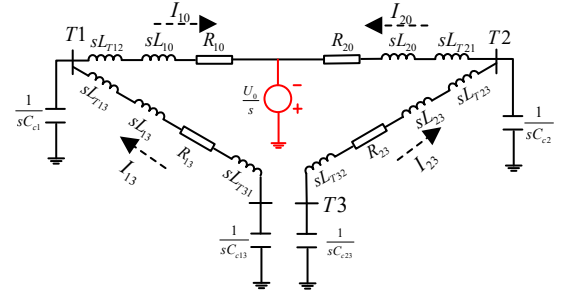

Fig. 3. Unlock meshed MTDC system into two independent radical networks.

approximate expression of $I_{10}(t)$ during the initial short period after fault. Based on the **Lemma 2** in the Appendix, in the high-frequency region, Z_{f10} in (5) can be regarded as a parallel connected DC-link capacitor for DC fault analysis, which is written as follows,

$$Z_{f10}{}^H(s) = 1/sC_{c1} \qquad (6)$$

Correspondingly, the high-frequency part of *Laplace Transform* of DC fault line current can be written as follows,

$$I_{10}{}^H(s) = \frac{U_0/s}{R_{10} + s(L_{10} + L_{T12}) + 1/sC_{c1}} \qquad (7)$$

Similarly, the fault current component of healthy line I_{13} can be written as follows,

$$I_{13}(s) = I_{10}(s) \cdot \frac{1/sC_{c1}}{s(L_{13} + L_{T13} + L_{T31}) + 1/sC_{c13} + 1/sC_{c1} + R_{13}} \qquad (8)$$

Then, the high-frequency part of *Laplace Transform* of DC healthy line current can be written as follows,

$$\begin{cases} I_{13}{}^H(s) = I_{10}{}^H(s) \cdot h(s) \\ h(s) = \dfrac{1}{s^2(L_{13} + L_{T13} + L_{T31})C_{c1} + (1+k)C_{c1}/C_{c3} + sR_{13}C_{c1} + 1} \end{cases} \qquad (9)$$

Equation (7) and (9) indicate the **high-frequency equivalent model** of three-terminal MTDC grid. Based on (7) and (9), the fault current component of healthy line equals to that of the fault line multiplied by $h(s)$. The transfer function $h(s)$ has the same characteristic of the second-order low-pass filter. In the perspective of the circuit analysis, the high-frequency fault components of the fault DC line will be bypassed through the paralleled connected capacitance of VSC. It is indicated that the high-frequency fault current components flow in the fault line and then dramatically decay in the healthy line.

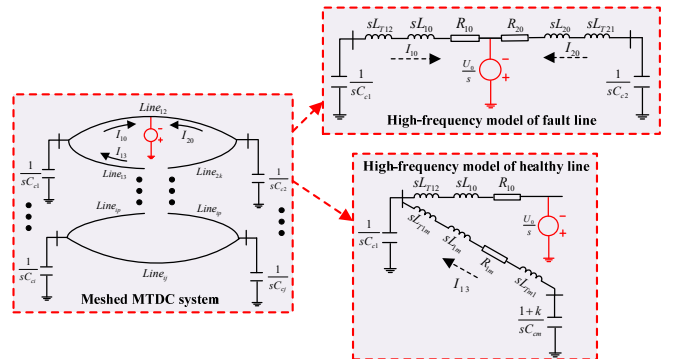The above analysis is applied to a three-terminal DC grid.

Fig. 4. High-frequency model of meshed MTDC system for fault current calculation.

For a general MTDC system, the high-frequency equivalent model as shown in Fig. 4 for the fault line and healthy line current calculation is written below,

$$\begin{cases} I_{10}^{H}(s) = \dfrac{U_0 / s}{R_{10} + s(L_{10} + L_{T12}) + 1/sC_{c1}} \\ I_{ij}^{H}(s) = I_{10}^{H}(s) \cdot \prod_{n=1}^{m} h_n(s) \end{cases} \quad (10)$$

The fault current component of healthy line equals to that of upper-level line multiplied by a low-pass filter $h_n(s)$.

Remarks: The influence of the correlated proportional coefficient (k) on the fault current calculation is rather limited since the two independent capacitors marked as C_{c13} and C_{c23} of VSC can be negligible in the high-frequency zone. In addition, with the increase of the DC terminals, DC lines that are far away from fault line can be regarded as constant current-source during initial period of the fault. Thus, meshed MTDC network is automatically decoupled by two independent circuits.

Ignoring the parallel connected capacitor of VSC as well as the branch resistance in the high-frequency region, the fault current component of Line 12 can be written as follows,

$$I_{10}^{H}(s) = \dfrac{U_0 / s}{s(L_{10} + L_{T12})} \quad (11)$$

Transforming (11) into time-domain expression, the fault line current during initial short period after fault can be expressed as follows,

$$I_{10}(t) = \dfrac{U_0}{L_{T12} + L_{10}} \cdot t \quad (12)$$

The proposed high-frequency equivalent model gives an important guidance for the model simplification if the initial stage of signal is more concerned for the system protection settings. In order to further simplify the expression in (9), based on the *Lemma 2* in the Appendix, only high-frequency part of $h(s)$, marked as $h^H(s)$ is reserved. Combine (9) and (11), the fault current component of Line 13 can be further simplified,

$$\begin{cases} h^{H}(s) = \dfrac{1}{s^2(L_{13} + L_{T13} + L_{T31})C_{c1}} \\ I_{13}^{H}(s) = I_{10}^{H}(s) \cdot h^{H}(s) = \dfrac{U_0}{s^4(L_{T12} + L_{10})(L_{13} + L_{T13} + L_{T31})C_{c1}} \end{cases} \quad (13)$$

Transforming (13) into time-domain expression, it can be given by the following equation,

$$I_{13}(t) = \dfrac{U_0}{6(L_{T12} + L_{10})(L_{13} + L_{T13} + L_{T31})C_{c1}} \cdot t^3 \quad (14)$$

(12) and (14) give an approximate fault current expression of fault line and healthy line based on the proposed high-frequency equivalent model, which effectively simplifies the original complex circuit for DC fault analysis. Thus, The initial fault current calculation of the fault DC line and healthy DC line can be reduced as a simplified RL and RLC circuit.

D. Fault current calculation with fault resistance

In the proposed high-frequency equivalent model, the parallel connected capacitors of VSC can be overlooked. Fig. 5 shows the simplified high-frequency equivalent circuit for fault current calculation of fault line with fault resistance R_f.
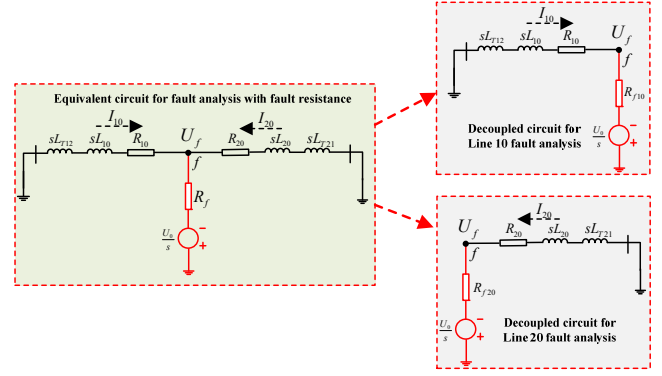

Fig. 5. Simplified high-frequency equivalent circuit for fault current calculation of fault line with fault resistance.

Similar to the analytical process of (2) and (3), the fault resistance R_f can be decoupled into two independent ones, marked as R_{f10}, R_{f20}, which belong to branch Line 10 and 20. The corresponding resistance should be satisfied as follows,

$$\begin{cases} R_{f10}(s) = \dfrac{(I_{10}(s) + I_{20}(s)) \cdot R_f}{I_{10}(s)} \\ R_{f20}(s) = \dfrac{(I_{10}(s) + I_{20}(s)) \cdot R_f}{I_{20}(s)} \end{cases} \quad (15)$$

As indicated by Fig. 5, the fault DC current of Line 10 and Line 20 can be expressed as follows,

$$\begin{cases} I_{10}(s) = \dfrac{U_f(s)}{s(L_{T12} + L_{10}) + R_{10}} \\ I_{20}(s) = \dfrac{U_f(s)}{s(L_{T21} + L_{20}) + R_{20}} \end{cases} \quad (16)$$

where, $U_f(s)$ is the DC-link voltage at the Point f as shown in Fig. 5. Based on the Equation (15) and (16), the corresponding resistance of R_{f10} and R_{f20} can be re-written as follows,

$$\begin{cases} R_{f10}(s) = \dfrac{s(L_{T12} + L_{T21} + L_{12}) + R_{10} + R_{20}}{s(L_{T12} + L_{10}) + R_{10}} \cdot R_f \\ R_{f20}(s) = \dfrac{s(L_{T12} + L_{T21} + L_{12}) + R_{10} + R_{20}}{s(L_{T12} + L_{20}) + R_{10}} \cdot R_f \end{cases} \quad (17)$$

Ignoring the branch resistance R_{10}, R_{20} in the high-frequency region, the (17) can be further reduced as follows,

$$\begin{cases} R_{f10} = \dfrac{L_{T21} + L_{12} + L_{T12}}{L_{T21} + L_{20}} R_f \\ R_{f20} = \dfrac{L_{T21} + L_{12} + L_{T12}}{L_{T12} + L_{10}} R_f \end{cases} \quad (18)$$

As shown in Fig.5, with the proposed high-frequency equivalent model, the fault Line 10 current calculation with fault resistance can be indicated by the following Equation:

$$I_{10}^{H}(s) = \dfrac{U_0 / s}{R_{10} + s(L_{10} + L_{T12}) + R_{f10}} \quad (19)$$

Ignoring the branch resistance R_{10} in the high-frequency region, the fault Line 10 current during the initial short period after fault can be expressed as follows,

$$\begin{cases} I_{10}(t) = \left(\dfrac{U_0}{R_{f10}} - \dfrac{U_0}{R_{f10}} \cdot e^{-t/\tau_1}\right) \cdot \varepsilon(t) \\ \tau_1 = (L_{10} + L_{T12}) / R_{f10} \end{cases} \quad (20)$$

where, τ_1 is the time constant of related *RL* circuit. It concerns with the fault location of the Line 12, the value of the fault resistance, and the inductance of the supplementary inductor.

III. PRIMARY PROTECTION SCHEME

A. Transient average value of current

Based on (12) and (14), it is validated that the fault current components of fault line increase linearly, while that of healthy line raises cubically during the initial period of DC fault. Therefore, it is crucial to find out an index that can be easily utilized to discriminate the fault DC line and healthy DC line in a fast and accurate manner. Transient average value of current is a basic feature of the transient current, which is defined as the mean value of transient fault DC current over a specific time period *T*. The continuous form can be written in (21).

$$\overline{f(t)} = \frac{1}{T}\int_{t-T}^{t} f(\tau) \cdot d\tau \qquad (21)$$

Selecting transient average value of transient signal as a protection indicator requires low computational burden and obtains high robustness to the outside noises compared to the traditional frequency based signal extraction methods such as *Fast Fourier Transform* (FFT) or *Wavelet Transform Method.*

B. Threshold value determination

In this part, the thresholds are determined to judge whether an event is a fault or not. The classical method to find the correct threshold values is conducting multiple simulations through a systematic search. By concentrating on the worst-case situations, the threshold value can be done in a relatively fast and straightforward manner. Considering the metallic fault happens at the beginning of the subordinate line of the protected line, and taking Line 12 for example, the transient fault current component should be expressed,

$$I_{12}(t) = \frac{U_0}{6L_{T23}(L_{12}+L_{T12}+L_{T21})C_{c2}} \cdot t^3 \qquad (22)$$

Accordingly, the transient average value of fault current component of Line 12, marked as $\overline{I}_{12}^{out}$ during the initial period after fault can be illustrated as follows,

$$\overline{I}_{12}^{out} = \frac{1}{T}\int_0^T I_{12}(t) \cdot dt = \frac{U_0}{24L_{T23}(L_{12}+L_{T12}+L_{T21})C_{c2}} \cdot T^3 \quad (23)$$

Therefore, the threshold value should be above the transient average value of Line 12 fault current, when the fault happens at the beginning of the Line 23,

$$I^{set} = m \cdot \overline{I}_{12}^{out} \qquad (24)$$

where *m* is the concerned coefficient. In this paper, in order to make sure the high-sensitivity of the proposed scheme, it is set as 20. The primary protection scheme is triggered if the following Equation is satisfied,

$$\overline{I}(t) > I^{set} \qquad (25)$$

C. Sensitivity analysis

When it comes to sensitivity analysis, the least sensitive metallic fault situation should be analyzed. Considering metallic fault happens at the end of Line 12, the transient average value of fault current component of Line 12, marked as $\overline{I}_{12}^{in}$ during the initial period after fault should be as follows,

$$\overline{I}_{12}^{in} = \frac{1}{T}\int_0^T I_{10}(t) \cdot dt = \frac{1}{T}\int_0^T \frac{U_0}{L_{12}+L_{T12}} t \cdot dt = \frac{U_0}{2(L_{12}+L_{T12})} \cdot T \quad (26)$$

Based on the definition of the sensitivity of the protection, the ratio of minimal transient average value of Line 12 and the set threshold value can be illustrated as follows,

$$K_{sen} = \frac{\overline{I}_{12}^{in}}{I^{set}} = \frac{12L_{T23}(L_{12}+L_{T12}+L_{T21})C_{c2}}{m(L_{12}+L_{T12}) \cdot T^2} > \frac{12L_{T23}C_{c2}}{m \cdot T^2} \quad (27)$$

where, K_{sen} is the sensitivity coefficient of the propose protection scheme, the DC-link capacitance of VSC is with several hundreds of μF, and the supplementary inductance at the beginning of the DC line is with several hundreds of mH. *m* is the concerned coefficient, defined as the ratio of the threshold value and the transient average value of Line 12 fault current, when the fault happens at the beginning of the Line 23. For the requirement of the sensitivity of the protection scheme and the length of the time window *T* should be satisfied as follows,

$$T < \sqrt{\frac{12L_{T23}C_{c2}}{m \cdot K_{sen}}} \qquad (28)$$

In order to guarantee the high-sensitivity of the proposed protection scheme, time window *T* in this paper is set as 2 ms, and the sensitivity indicator K_{sen} is larger than 10, which makes sure the high sensitivity of the proposed protection scheme.

D. Complexity of the proposed method

For the transient average value of fault current component $\overline{I}_{12}(j)$ during the specific time window *T* in the discrete form can be illustrated as follows,

$$\overline{I}_{12}(j) = \frac{1}{N}\sum_{i=j}^{i=j+N-1} I_{12}(i) \qquad (29)$$

where, *N* is the sampling number during the time window *T*, and $Nf_s=T$ is satisfied. For the next successive transient average values of fault current component marked as $\overline{I}_{12}(j+1)$ can be expressed as follows,

$$\overline{I}_{12}(j+1) = \frac{1}{N}\sum_{i=j+1}^{i=j+N} I_{12}(i) \qquad (30)$$

Combine (29) and (30), following expression should be held,

$$\overline{I}_{12}(j+1) = \frac{1}{N}\sum_{i=j}^{i=j+N-1} I_{12}(i) + \frac{1}{N}(I_{12}(j+N)-I_{12}(j))$$
$$= \overline{I}_{12}(j) + \frac{1}{N}(I_{12}(j+N)-I_{12}(j)) \qquad (31)$$

Equation (31) indicates the proposed method only involves two times addition and one times multiplication operations. Compared with the traditional *Fast Fourier Transform* (FFT) method [18] that includes $N\log_2 N$ times complex addition and $N/2\log_2 N$ times complex multiplication operation in a computational cycle, the proposed transient average value based method is sufficiently simple and well suitable for the industrial application.

E. Startup program for the proposed protection scheme

In order to achieve fast fault identification, the primary

protection scheme should be initiated by the start up element for checking every possible fault quickly. When a DC fault happens, the faults can be characterized by a increasing current magnitude. Taking Line 12 as an example, a current derivation criterion can be employed for the startup element of the primary protection, which can be written in a discrete form as follows:

$$\left| I_{12}(j+1) - I_{12}(j) \right| > \Delta I_{12set} \tag{32}$$

where, ΔI_{12set} is the threshold value for the startup element of the protection. The value should be higher than the maximal load current changes, which is indicated by ΔI_{Lmax}. Meanwhile, The startup element should be activated under the high fault resistance grounded situation, so the threshold value should be less than fault current change of Line 12 under the maximal tolerant fault resistance. Based on the Equation (20), the fault current change of Line 12 marked as ΔI_{12r} during one sampling cycle can be expressed as follows,

$$\Delta I_{12r} = \frac{U_0}{R_{f10}} \cdot (1 - e^{-\frac{1}{f_s \tau_1}}) \tag{33}$$

Therefore, the threshold value for the startup element of the protection can be determined based on the following inequality constraints:

$$\eta \cdot \Delta I_{Lmax} < \Delta I_{12set} < \zeta \cdot \Delta I_{12r} \tag{34}$$

where, η and ζ are two concerned coefficients for ensuring the reliability of the startup element of the protection scheme. η is larger than 1, and ζ is in a range of $(0, 1)$. The flowchart of the proposed protection scheme can be referred as Fig. 6.

F. High fault resistance tolerance ability

Based on (20), considering a fault happens at the end of the Line 12, the transient average value of line current can be written in (35).

$$\overline{I}_{12} = \frac{1}{T}\int_0^T I_{10}(t) \cdot dt = \frac{1}{T}\int_0^T (\frac{U_0}{R_{f10}} - \frac{U_0}{R_{f10}} \cdot e^{-t/\tau_1}) \cdot dt$$
$$= \frac{U_0}{R_{f10}}(1 - \frac{\tau_1}{T}) + \frac{U_0}{R_{f10}} \cdot \frac{\tau_1}{T} \cdot e^{-T/\tau_1} \tag{35}$$

In order to analyze the attenuation of the transient current caused by the increase of fault resistance, the decay coefficient ρ is defined as follows,
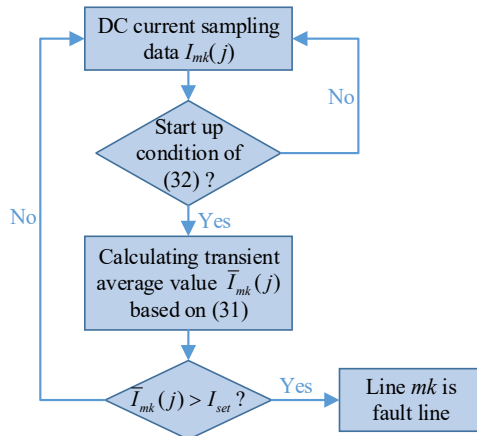

Fig. 6. Overall flow chat of the primary protection schemes for MTDC system.

$$\rho = \frac{\overline{I}_{12}}{I_{12}^{in}} = \frac{2\tau_1}{T} \cdot (1 - \frac{\tau_1}{T}) + \frac{2\tau_1^2}{T^2} e^{-T/\tau_1} \tag{36}$$

As the fault resistance R_{f10} increases, the time constant τ_1 decreases, and consequently, ρ will decrease. Normally for a 300 km transmission line, the inductance of DC line will be 4~5 times of the supplementary inductance at the terminal of DC line. Considering fault resistance $R_f=500\Omega$, the time constant value τ_1 is around 0.17ms for a 300 km DC transmission line, then (36) becomes as follows,

$$\rho|_{R_f=500\Omega} > \frac{2\tau_1}{T} \cdot (1 - \frac{\tau_1}{T})$$
$$= 0.2857 \times (L_{12} + L_{T12})(1 - 0.1429 \times (L_{12} + L_{T12})) \tag{37}$$
$$\approx 0.155$$

For a 300 km transmission DC line, the decay coefficient for fault resistance $R_f=500\Omega$ is larger than 0.15. It is well indicated that the proposed method has high tolerance to fault resistance.

IV. ERROR EVALUATION BETWEEN DISTRIBUTED PARAMETER LINE MODEL AND LUMPED PARAMETER LINE MODEL

When analyzing the transient process of MTDC grid during initial period after fault, the distributed parameter line model should be utilized. Transient current travelling-wave appears in the fault DC line, which impedes the above analytical method based on the lumped parameter model. When the fault happens in the meshed MTDC, it is regarded as a square-wave pulse generated from fault location and travelling among the entire system. Base on the Peterson's law, the first injection of current travelling-wave $I_{12t,1}$ when encountering the supplementary inductor at the beginning of Line 12 is expressed as follows,

$$I_{12t,1} = \frac{2U_0}{Z_l} - \frac{2U_0}{Z_l} \cdot e^{-t/\tau_2} \tag{38}$$

where, L_0 and C_0 are the line inductance and capacitance per-meter. $Z_l = \sqrt{L_0/C_0}$ is the wave impedance of current travelling wave, and it is normally as 400-500Ω. τ_2 is the time constant of current travelling wave, and can be expressed,

$$\tau_2 = L_{T12}/Z_l \tag{39}$$

τ_2 is around 0.2ms when L_{T2} is selected as 100mH. When the fault happens at the end of the long transmission line, the transient process of first injection current travelling-wave expressed by (38) is finished and the change of the fault line current ΔI_{12D} during the specific time period T can be obtained,

$$\Delta I_{12D} = \frac{2U_0}{Z_l} = \frac{2U_0}{L_0 \cdot v} \tag{40}$$

where, v is the speed of travelling wave, and equals to $(L_0 C_0)^{1/2}$. The time window T equals the time when the second injection of current travelling-wave comes at the beginning of Line 12,

$$T = 2l/v \tag{41}$$

Based on (12), when using the lumped parameter line model, the change of the fault line current ΔI_{12L} during the specific time period T is expressed as follows,

$$\Delta I_{12L} = \frac{U_0}{(L_0 + L_{T2}/l)l} \cdot \frac{2l}{v} \tag{42}$$

Therefore, based on (40) and (42), the ratio of the change of the fault line current during time period T with different line models is shown below,

$$\frac{\Delta I_{12L}}{\Delta I_{12D}} = \frac{L_0}{L_0 + \frac{L_{T2}}{l}} \tag{43}$$

It can be concluded that the ratio will gradually increase with the increase length of DC line. For a 300 km DC line, the ratio is calculated around 0.83. The above analysis is suitable for the first injection of current travelling-wave. However, for the several injections and reflections of current travelling-wave, it is hard to obtain the analytical expression. In addition, the travelling-wave effects are dramatically mitigated by several injections and reflections of current travelling-wave, and the fault current with two line models are nearly the same.
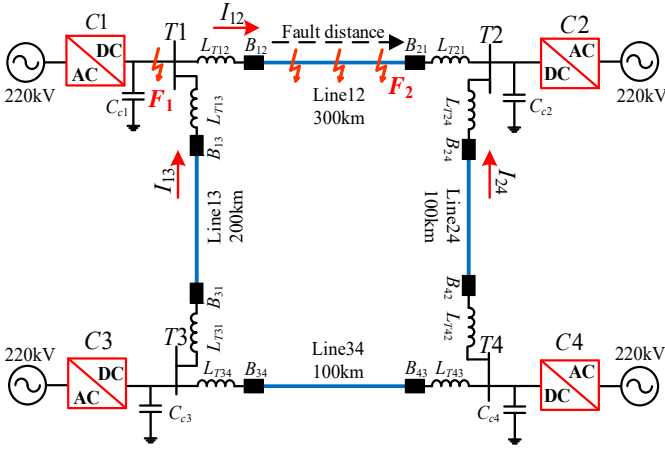

Fig. 7. The outline of the studied four-terminal DC grid.

V. SIMULATION STUDIES

In order to validate the effectiveness of the proposed protection scheme, a four-terminal HVDC grid [15] modeled in PSCAD/EMTDC is shown in Fig. 7. The DC reactors of 100mH are implemented at each end of DC overhead lines. The capacitance of VSC capacitor and the short circuit ratios (SCR) of equivalent AC systems are provided in Table I. Each VSC with the detailed switching model is connected through DC lines with frequency dependent (FD) representation. Converter station $C1$, $C3$, and $C4$ are in active and reactive control model [16], while the converter station $C2$ controls DC-link voltage and the exchanged reactive power with the connected AC grid. The time window T is set to 2ms in this paper. Based on (23) and (24), the threshold value for the primary protection scheme I_{12}^{set} and I_{24}^{set} are set to 0.0242kA and 0.0459kA, respectively. The sampling frequency f_s is selected as 10 kHz in the paper.

A. Model verification and threshold calculation

Fig. 8 shows the simulation results when the metallic fault happens at the end of Line 12 (fault distance d=300km). Three different models with lumped parameter of DC line (RL model), with frequency dependent (FD) model of DC line, and with the proposed high-frequency (HF) equivalent model are compared in Fig. 8. It is clearly seen from Fig. 8 (a) that with FD model, the travelling-wave effects appear in Line 12, and

TABLE I
PARAMETERS OF TEST MTDC SYSTEM

Symbol	Item	Value
C_{ci}	Capacitor of VSC	880 µF
L_{Tij}	Supplementary Inductance	100 mH
L_0	Inductance per kilometer of DC line	1.635 mH
SCR	AC side system SCR	5.6
f_s	Sampling frequency	10 kHz
T	Time window in a cycle	2 ms
R_0	Resistance per kilometer of DC line	0.015 Ω
Z_l	wave impedance of travelling wave	490 Ω
I_{12}^{set}	Threshold value for Line 12	0.0242 kA
I_{24}^{set}	Threshold value for Line 24	0.0459 kA

the fault current begins to surge suddenly when the first injection of current travelling-wave comes at L_{T12}, located at the beginning of Line 12 at t=1.001s. With RL model, the fault current curve that increases smoothly at t=1s is very similar to that with the proposed high-frequency model. It is well verified that when analyzing the transient process during the initial period after fault, the complex DC circuit network can be simplified as the high-frequency part of the original network with relatively high-accuracy. Although the fault current component of Line 12 with two line models (FD model and RL model) are different as shown in Fig. 8 (a), the transient average values of them are quite similar shown in Fig. 8 (b). With FD model, the transient average value of Line 12 current exceeds
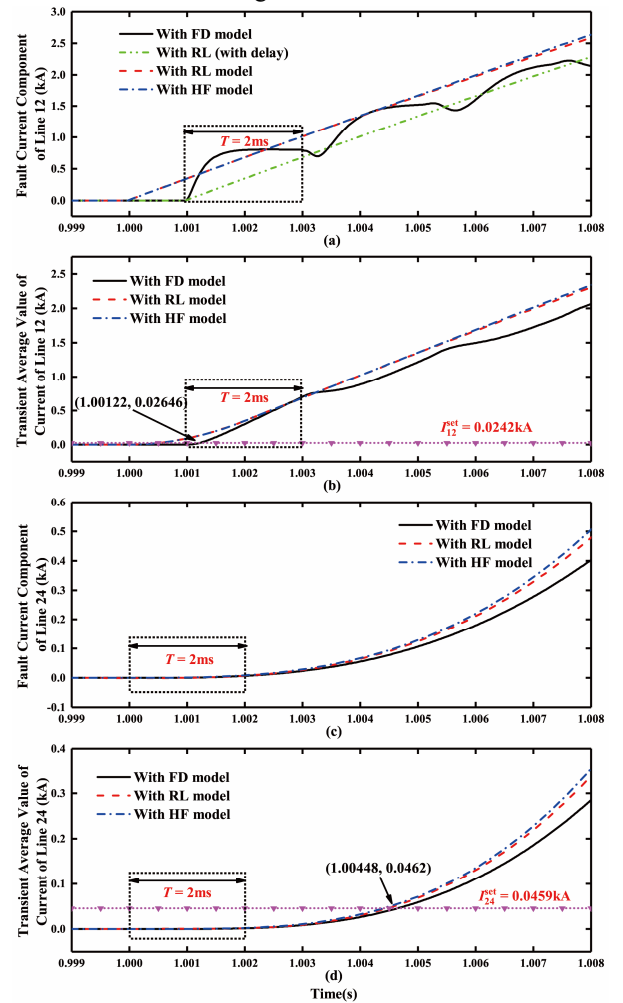

Fig. 8. Simulation results with different models.

the threshold value at t=1.0012 ms. Fig. 8 (c) and (d) indicate that there is no travelling-wave effects in the healthy line (Line 24), which leads to the fault current component curves of healthy line very similar based on three different line models. It can be seen from Fig. 8 (d) that the transient average values of Line 24 with all three models are far less than the set threshold value within 4 ms after DC fault, which guarantees the high-sensitivity of the proposed protection scheme.

B. Influence of fault location

Table II shows the fault current component of fault line and healthy line with different fault locations under T=2ms. It is clearly seen that the transient average value of fault line current increases with decrease of fault locations. In addition, the transient average value with three line models are quite similar, which is far larger than the threshold value. For the healthy Line 24, the transient average value of current decreases with the decrease of fault locations. However, for the healthy Line 13, the transient average value of current increases with the decrease of fault locations. The ratio of transient average value of fault line and healthy line current is above 250, which verifies the high-sensitivity of primary protection scheme.

Fig. 9 shows the transient average value of fault current component of Line 12 and Line 24 when the metallic fault
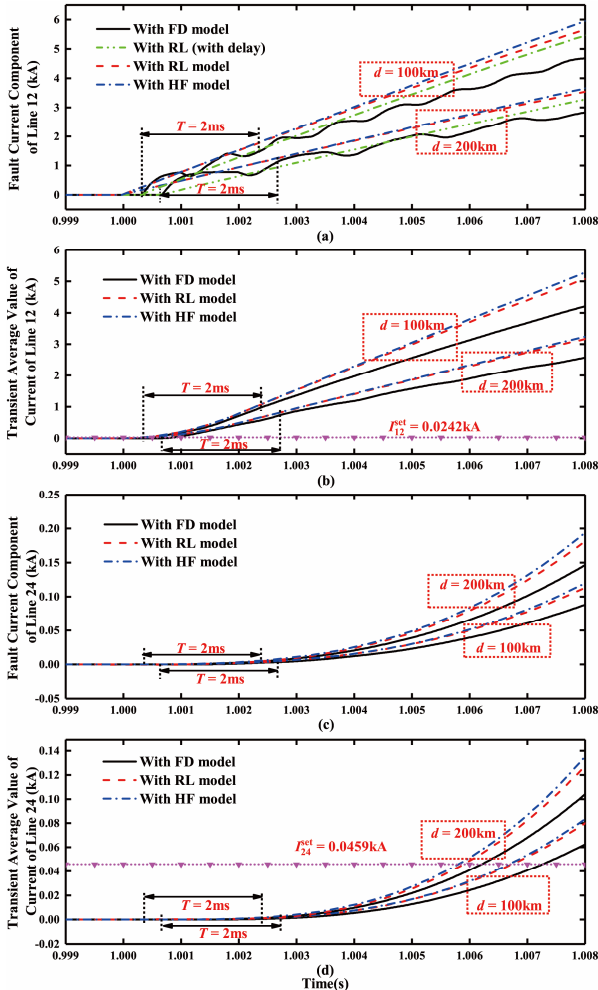

Fig. 9. Simulation results with different models under different fault locations.

TABLE II
INFLUENCE OF FAULT LOCATIONS ON THE PROTECTION SCHEME

Fault Location (km)	Transient average value of fault line (Line 12) kA		
	FD model	RL model	HF model
300	0.708	0.699	0.699
250	0.710	0.771	0.772
200	0.744	0.823	0.828
150	0.836	0.904	0.910
100	0.941	1.035	1.043
50	1.118	1.304	1.295
Fault Location (km)	Transient average value of healthy line (Line 24) kA		
	With FD model	With RL model	With HF model
300	0.00166	0.00185	0.00233
250	0.00158	0.00169	0.00203
200	0.00152	0.00154	0.00185
150	0.00126	0.00141	0.00158
100	0.00107	0.00122	0.00149
50	0.00097	0.00113	0.00136
Fault Location (km)	Transient average value of healthy line (Line 13) kA		
	With FD model	With RL model	With HF model
300	0.000606	0.000654	0.000666
250	0.000862	0.000863	0.000873
200	0.00109	0.00110	0.00113
150	0.00132	0.00139	0.00144
100	0.00168	0.00171	0.00179
50	0.00190	0.00205	0.00217

happens at 100 km and 200 km away from the beginning of the Line 12. Fig. 9 (a) shows the change of fault current component of Line 12 with FD model and with RL model are nearly the same within the selected time windows. In addition, it shows that high-frequency equivalent model has high-accuracy compared to the RL model within short-time period, as illustrated in Fig. 9 (a) and (c). As is shown in Fig. 9 (b), the transient average value of Line 12 current with FD model is nearly linear, and the traveling-wave effects can be neglected when the fault distance is short.

C. Influence of fault resistance

TABLE III
INFLUENCE OF FAULT RESISTANCES ON PROPOSED SCHEME

Fault Location (d =300km)	Transient average value of fault line (Line 12) kA		
	100 Ω (0.5 p.u.)	200 Ω (1.0 p.u.)	500Ω (2.5 p.u.)
FD model	0.337	0.219	0.0882
RL model	0.258	0.144	0.0680
HF model	0.256	0.142	0.0675
Fault Location (d =200km)	Fault current component of fault line (Line 12) kA		
	100 Ω (0.5 p.u.)	200 Ω (1.0 p.u.)	500Ω (2.5 p.u.)
FD model	0.470	0.339	0.1762
RL model	0.485	0.324	0.1520
HF model	0.488	0.326	0.1491

Table III compares the transient average value of fault line current under different fault resistances with different models involved under time window T=2ms. It can be clearly seen that with the increase of the fault resistances, the transient average value is decreasing. As shown in Fig. 10, with high fault resistance at the end of Line 12, the fault current component with FD model has apparent oscillation. This characteristic makes the error of transient average value of Line 12 with FD model and RL model relatively large as shown in Table III. However, as the travelling-wave gradually decays after several injections and reflections, the transient average value with FD model and that with RL model are gradually the same as shown in Fig. 10 (a) and (c). In the initial short period after fault, the

fault current component of Line 12 with RL model and that with the proposed HF model are very similar under different fault resistances, which again verifies the validity of HF model. With FD model, the transient average value of Line 12 current is 0.0882kA when the fault occurs at the end of Line 12 with 500 Ω fault resistance, which is larger than the threshold set as 0.0242kA. Simulation results show that the proposed protection scheme can tolerant 2.5 p.u. fault resistance.
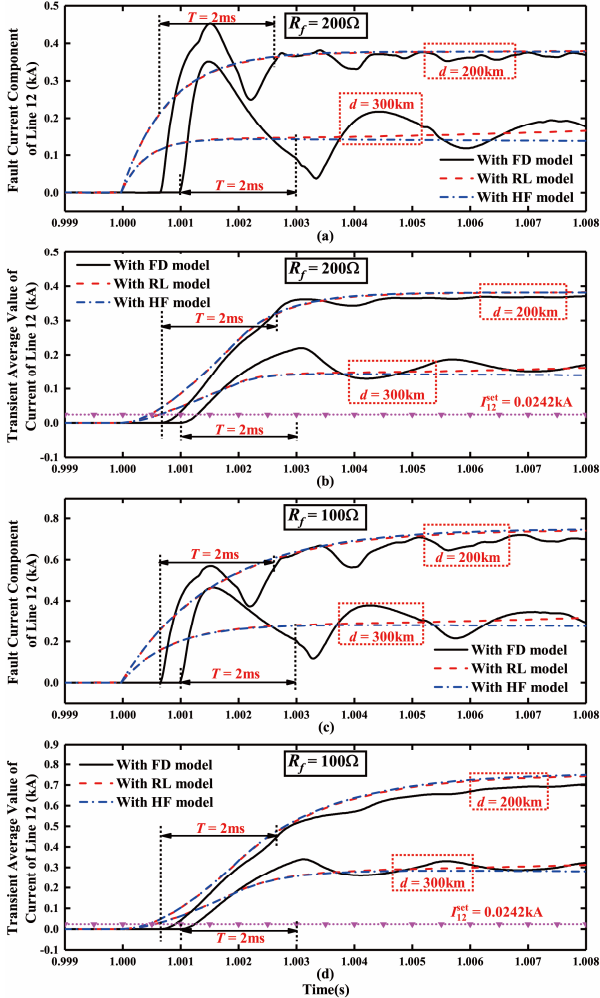

Fig. 10. Simulation results under different fault resistances.

D. Protection coordination for external fault

In the fault location marked as F_1 (before the terminal inductance and after the capacitor), the fault can be cleared quickly by the converter protection. For instance, by detecting the DC current difference before the terminal inductance and after the capacitor, the fast current differential protection can be realized. If the value is larger than the set threshold, the DC CB B_{12} and B_{13} will be switched out quickly to isolate the fault. If the former protection level (converter protection) cannot be initiated, additional directional component and communication should be included to make sure the reliability of the proposed protection scheme. For the fault happens at F_1, B_{12} and B_{13} will not be switched off since the fault direction is inverse. Meanwhile, B_{12} and B_{13} will send the blocking signal to the other side of the breaker immediately to inform the B_{21} and B_{31}

keeping connected since it is the external fault so that the fast primary protection of DC lines will not be activated.

However, if the fault F_1 still prevails, the fault should be isolated to make sure the system cannot be entirely out of operation. The fast line protection can be settled as a back-up protection of the previous level protection of converter by delaying some milliseconds of operation of B_{21} and B_{31}. Fig.11 shows the simulation results when the metallic fault happens at F_1, and it is clearly seen that B_{12} is blocked since the measured transient average value of fault current $\bar{I}_{12}$ is negative, and it is a backward fault. As shown in Fig.11 (b), when the transient average value of $\bar{I}_{21}$ exceeds the threshold at t=1.0014s, B_{21} keep connected since it has already received the blocking signal sent by B_{12}. After a proper time delay of 3 ms set in the paper, if the transient average value $\bar{I}_{21}$ is still above the set threshold, B_{21} can be switched off to make sure the fault isolation of F_1.
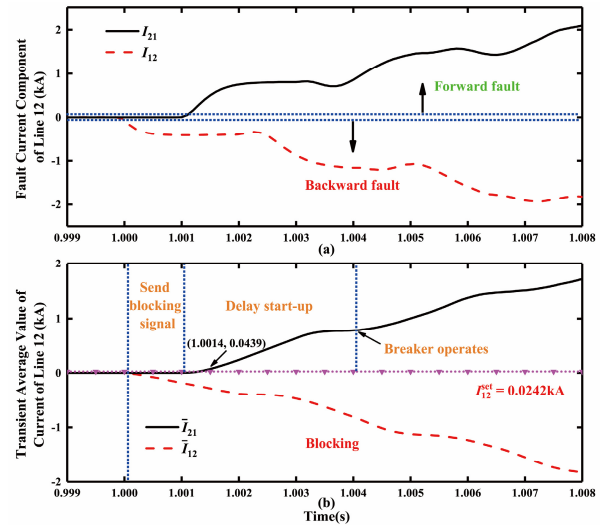

Fig. 11. Simulation results when a metallic fault happens at F_1.

E. Comparison with ROCOC based protection method

Fig. 12 compares the performance of different DC fault detection methods (proposed transient average value of current and rate of change of current (ROCOC) based method) with relatively low sampling frequency at 5 kHz under different fault resistances. With the metallic fault, the rate of change of Line 12 current has high value when the first injection of current traveling wave arrives at the inductance terminal at t=1.001s, which verifies the high-sensitivity of the ROCOC method for DC fault detection. However, the ROCOC value decreases dramatically with the time. The fourth and fifth ROCOC value comes to 0.24 and 0.1 as shown in Fig. 12 (a), and is vulnerably below the set threshold. In addition, when the sampling frequency is further decreasing, or missing the first few data of initial DC fault current, the primary protection based on ROCOC becomes invalid. However, the transient average value of Line 12 with 5 kHz sampling frequency is almost the same as that with 10 kHz sampling frequency. In addition, as depicted in Fig. 12 (b), missing of some initial current data does not affect the accurate action of the proposed protection scheme. With 300Ω fault resistance, the transient travelling wave fast decays as shown in Fig. 12 (c). The difference between third
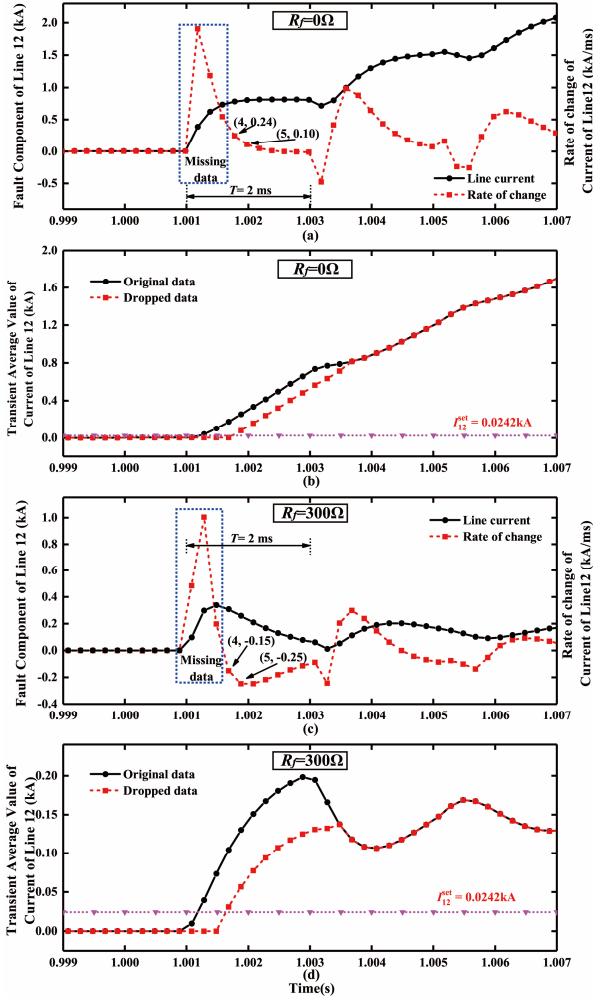
Fig. 12. Simulation results with different protection schemes under different fault resistances.

and fifth sampling point of fault component of Line 12 is very small, which might result in the primary protection based on ROCOC invalid. However, the transient average value of Line 12 under 5 kHz sampling frequency with initial current data missing can still make sure the accurate action of the primary protection scheme as shown in Fig. 12 (d), which verifies the high robustness of the proposed protection scheme.

VI. CONCLUSION

This paper firstly proposes a high-frequency equivalent model of VSC-MTDC system for fault current calculation during initial short period after fault. Accordingly, a novel DC fault detection method for VSC based MTDC system that utilizes the transient average value of line current is further proposed. In the scheme, the fault line can be identified fast with one-end signal. In addition, the influence of transient travelling-wave on the proposed protection scheme is also investigated, which indicates the transient travelling-wave on the fault line has very limited impact on the accurate operation of proposed primary protection. Numerous simulation studies have demonstrated that the proposed high-frequency equivalent model can be utilized for fault analysis of MTDC system and the proposed scheme is effective under different fault locations

and high fault resistances. Compared with the traditional protection schemes based on ROCOC, the proposed one stands out for relatively low sampling frequency, low computational burden, high fault resistance tolerant ability, and high robustness with respect to the data missing.

APPENDIX

Define *Discrete Fourier Transform* (DFT) of fault line DC current, it yields as follows,

$$X(k) = \sum_{n=0}^{N-1} I_{10}(n) \cdot e^{-j\frac{2\pi}{N}kn} \tag{A.1}$$

where $X(k)$ is the DFT of the fault line DC current. N is the sampling number in a time period of T. Rewrite (A.1) in a continuous form, which is given by:

$$X'(k) = \frac{X(k)}{N} = \frac{1}{N}\sum_{n=0}^{N-1} I_{10}(n)e^{-j\frac{2\pi}{N}kn} \approx \frac{1}{T}\int_0^T I_{10}(t)e^{-j\frac{2\pi}{T}kt}dt \tag{A.2}$$

where $X'(k)$ is the *Discrete Fourier Series* of (5).

Lemma 1: DFT of the continuous aperiodic signal $f(t)$ equals to the polynomial function times the *Fourier Transform* of $f(t)$ on the condition that the sampling time T is short enough.

Proof: The general format of *Continuous Fourier Series* can be written as follows,

$$G(\omega, T) = \frac{1}{T}\int_0^T f(t) \cdot e^{-j\omega t} \cdot dt \tag{A.3}$$

Considering the small sampling time of T and $f(0)=0$, $f(t)$ can be expressed as follows by using *Taylor Series* around zero,

$$f(t) = f(0) + f'(0)\cdot t + f''(0)/2 \cdot t^2 + \cdots \approx f^{(m)}(0)\cdot t^m / m! \tag{A.4}$$

where, m is the least positive integer subject to $f^{(m)}(0)\neq 0$.

Combining (A.3) and (A.4), based on $e^{-j\omega T}=1$, the following expression can be hold,

$$G(\omega, T) \approx \frac{1}{T}\int_0^T f^{(m)}(0)t^m/m!e^{-j\omega t}dt = \sum_{i=1}^{m} -\frac{T^{m-i}f^{(m)}(0)}{(j\omega)^i(m+1-i)!} \tag{A.5}$$

Considering the *Classical Fourier Transform* of $f(t)$,

$$F(\omega) = \int_0^\infty f(t)e^{-j\omega t}dt \approx \int_0^\infty f^{(m)}(0)t^m/m!e^{-j\omega t}dt = \frac{f^{(m)}(0)}{(j\omega)^{m+1}} \tag{A.6}$$

Based on (A.5) and (A.6), the following expression can be obtained,

$$G(\omega, T) \approx -\sum_{i=1}^{m} \frac{T^{m-i}\cdot(j\omega)^{m+1-i}\cdot F(\omega)}{(m+1-i)!} \tag{A.7}$$

Rewrite (A.7) in a *Laplace Form* and based on (A.2),

$$X(k) = N\cdot G(\omega, T) = -N\sum_{i=1}^{m}\frac{T^{m-i}\cdot s^{m+1-i}}{(m+1-i)!}L(f(t))_{s=\omega\cdot j} = \Gamma(s)\cdot L(f(t)) \tag{A.8}$$

where, $\Gamma(s)$ is the defined polynomial function.
END

Lemma 2: The continuous aperiodic signal $f(t)$ equals to the *Inverse Laplace Transform* of high-frequency part of the *Laplace Transform* of $f(t)$ during the initial period of the signal.

Proof: Suppose $X(k)$ is the DFT of the aperiodic signal $f(t)$, the following expression should be hold as follows:

$$X(k) = \Gamma(s)\cdot L(f(t))_{s=k\cdot\frac{2\pi}{N}f_s\cdot j} \tag{A.9}$$

where, f_s is the sampling frequency. The frequency interval of $X(k)$ marked as Δf can be expressed as follows,

$$\Delta f = f_s / N = 1/T \qquad (A.10)$$

When the sampling cycle T is small, the frequency interval will be large enough, and DFT of the aperiodic signal $f(t)$ is approximately as follows,

$$X(k) = \Gamma(s) \cdot L(f(t))_{s=k \cdot \frac{2\pi}{N} f_s \cdot j} \approx \Gamma(s) \cdot L^H(f(t))_{s=k \cdot \frac{2\pi}{N} f_s \cdot j} \qquad (A.11)$$

where, $L^H(f(t))$ is the high-frequency component of *Laplace Transform* of the signal $f(t)$. Define another continuous aperiodic signal $g(t)$, which can be expressed as follows,

$$g(t) = L^{-1}(L^H(f(t))) \qquad (A.12)$$

The DFT of the aperiodic signal $g(t)$ should satisfy below,

$$DFT(g(t)) = \Gamma(s) \cdot L^H(f(t))_{s=k \cdot \frac{2\pi}{N} f_s \cdot j} \approx DFT(f(t)) \qquad (A.13)$$

Based on (A.12) and (A.13), the following equation is hold,

$$f(t) \approx g(t) = L^{-1}(L^H(s)) \qquad (A.14)$$

END

REFERENCES

[1] R. Shah, J. C. Sánchez, R. Preece and M. Barnes, "Stability and control of mixed AC–DC systems with VSC-HVDC: a review," *IET Generation, Transmission & Distribution*, vol. 12, no. 10, pp. 2207-2219, 5 29 2018.

[2] Y. Li, Z. Xu, J. Østergaard and D. J. Hill, "Coordinated Control Strategies for Offshore Wind Farm Integration via VSC-HVDC for System Frequency Support," *IEEE Transactions on Energy Conversion*, vol. 32, no. 3, pp. 843-856, Sept. 2017.

[3] MacIlwain C. Energy: supergrid. Nature 2010;468(7324):624–5.

[4] P. Han and S. Wang, "Parameter coordination of modular multilevel converter for robust design during DC pole to pole fault," *Proc. China Int. Conf. Elect. Distrib*., 2012, pp. 1–5.

[5] J. Yang, J. E. Fletcher and J. O'Reilly, "Short-Circuit and Ground Fault Analyses and Location in VSC-Based DC Network Cables," *IEEE Transactions on Industrial Electronics*, vol. 59, no. 10, pp. 3827-3837, Oct. 2012.

[6] J. Rafferty, L. Xu, and D. J. Morrow, "DC fault analysis of VSC based multi-terminal HVDC systems, " *Proc. IET Int. Conf. AC DC Power Transmiss*., Birmingham, U.K., 2012, pp. 1–6.

[7] Z. Zhang and Z. Xu, "Short-circuit current calculation and performance requirement of HVDC breakers for MMC-MTDC systems, " *IEEJ Trans. Elect. Electron. Eng*., vol. 11, no. 2, pp. 168–177, Mar. 2016.

[8] C. Li, C. Zhao, J. Xu, Y. Ji, F. Zhang and T. An, "A Pole-to-Pole Short-Circuit Fault Current Calculation Method for DC Grids," *IEEE Transactions on Power Systems*, vol. 32, no. 6, pp. 4943-4953, Nov. 2017.

[9] J. Descloux, P. Rault, S. Nguefeu, J. B. Curis, X. Guillaud, F. Colas, et al., "HVDC meshed grid: Control and protection of a multi-terminal HVDC system," CIGRE, 2012.

[10] J. Sneath and A. D. Rajapakse, "Fault Detection and Interruption in an Earthed HVDC Grid Using ROCOV and Hybrid DC Breakers," *IEEE Transactions on Power Delivery*, vol. 31, no. 3, pp. 973-981, June 2016.

[11] Z. Zheng, T. Tai, J. S. Thorp and Y. Yang, "A Transient Harmonic Current Protection Scheme for HVDC Transmission Line," *IEEE Transactions on Power Delivery*, vol. 27, no. 4, pp. 2278-2285, Oct. 2012.

[12] G. Li, J. Liang, F. Ma, C. E. Ugalde-Loo and H. Liang, "Analysis of Single-Phase-to-Ground Faults at the Valve-Side of HB-MMCs in HVDC Systems," *IEEE Transactions on Industrial Electronics*, vol. 66, no. 3, pp. 2444-2453, March 2019.

[13] F. Kong, Z. Hao, S. Zhang, and B. Zhang, "Development of a novel protection device for bipolar HVDC transmission lines," *IEEE Transactions on Power Delivery*., vol. 29, no. 5, pp. 2270–2278, Oct. 2014.

[14] J. Beerten, S. Cole, and R. Belmans, "Modeling of Multi-Terminal VSC HVDC Systems With Distributed DC Voltage Control," *IEEE Transactions on Power Systems*, vol. 29, pp. 34-42, Jan 2014.

[15] R. Li; L. Xu; L. Yao, "DC Fault Detection and Location in Meshed Multi-terminal HVDC Systems Based on DC Reactor Voltage Change Rate," *IEEE Transactions on Power Delivery*., vol.32, no.3, pp. 1516-1526, June 2017.

[16] C. Li, A. M. Gole and C. Zhao, "A Fast DC Fault Detection Method Using DC Reactor Voltages in HVDC Grids," *IEEE Transactions on Power Delivery*. to be published.

[17] J. Liu, N. Tai and C. Fan, "Transient-Voltage-Based Protection Scheme for DC Line Faults in the Multiterminal VSC-HVDC System," *IEEE Transactions on Power Delivery*, vol. 32, no. 3, pp. 1483-1494, June 2017.

[18] K. Satpathi, Y. M. Yeap, A. Ukil and N. Geddada, "Short-Time Fourier Transform Based Transient Analysis of VSC Interfaced Point-to-Point DC System," *IEEE Transactions on Industrial Electronics*, vol. 65, no. 5, pp. 4080-4091, May 2018.

Yujun Li (S'15) received his B.Sc and M.Sc degrees from Xi'an Jiaotong University, China, in 2011, and Zhejiang University, China, in 2014 in Electrical Engineering, respectively. He received the Ph.D degree in Hong Kong Polytechnic University in 2017. From 2017 to now, he is a lecturer in Xi'an Jiaotong University, China. His main fields of interest include grid integration of renewable energy and HVDC modeling, fault analysis and detection of power systems.

Jiapeng Li received the B.Eng. degree in electrical engineering from Xi'an Jiaotong University, Xi'an, China, in 2017, and is currently pursuing the Ph.D. degree at Xi'an Jiaotong University. His research interests include protection and fault location of HVDC system.

Liansong Xiong (S'12-M'16) was born in Sichuan, China, in 1986. He received B.S., M.S. and Ph.D. degrees in Electrical Engineering from Xi'an Jiaotong University (XJTU), in 2009, 2012 and 2016, respectively. In June 2016, he joined the Nanjing Institute of Technology (NJIT), introduced in High-Level Academic Talent Plan of NJIT. Since November 2017, he is with the Department of Electrical Engineering, Hong Kong Polytechnic University, as a Research Associate. His research interests are power quality, multilevel converter, renewable energy, stability analysis, etc.
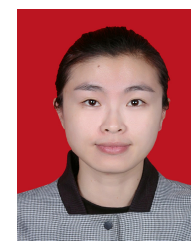
Xian Zhang received the B.Sc. degree from North China Electric Power University, China, in 2009, the M.Sc. degree from Tsinghua University, China, in 2012, and the Ph.D. degree from The Hong Kong Polytechnic University, in 2019, all in electrical engineering. Her main fields of interest include smart grid and electric vehicle.
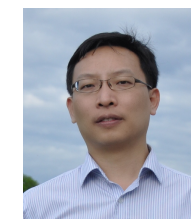
Zhao Xu (M'06–SM'13) received the Ph.D. degree in electrical engineering from The University of Queensland, Brisbane, Australia, in 2006.From 2006 to 2009, he was an Assistant and later Associate Professor with the Centre for Electric Technology, Technical University of Denmark, Lyngby, Denmark. Since 2010, he has been with Hong Kong Polytechnic University. His research interests include demand side, grid integration of wind power, electricity market planning and management, and AI applications. He is an Editor of the Electric Power Components and Systems journal.